AGU PUBLICATIONS

JGR

Journal of Geophysical Research: Atmospheres

RESEARCH ARTICLE
10.1002/2016JD024936

Key Points:
- Changes in TC intensification during the premonsoon months of May-June in the Bay of Bengal resemble a meridional dipole
- These changes in TC activity are consistent with those in the environment that suggest a strengthening of May-June monsoon circulation
- Decadal changes in ENSO impacted premonsoon Bay of Bengal TC activity through remote teleconnection mechanisms

Supporting Information:
- Supporting Information S1

Correspondence to:
K. Balaguru,
Karthik.Balaguru@pnnl.gov

Citation:
Balaguru, K., L. R. Leung, J. Lu, and G. R. Foltz (2016), A meridional dipole in premonsoon Bay of Bengal tropical cyclone activity induced by ENSO, *J. Geophys. Res. Atmos.*, *121*, 6954–6968, doi:10.1002/2016JD024936.

Received 11 FEB 2016
Accepted 6 JUN 2016
Accepted article online 10 JUN 2016
Published online 30 JUN 2016

A meridional dipole in premonsoon Bay of Bengal tropical cyclone activity induced by ENSO

Karthik Balaguru[1], L. Ruby Leung[2], Jian Lu[2], and Gregory R. Foltz[3]

[1] Marine Sciences Laboratory, Pacific Northwest National Laboratory, Seattle, Washington, USA, [2] Atmospheric Sciences and Global Change, Pacific Northwest National Laboratory, Richland, Washington, USA, [3] Physical Oceanography Division, Atlantic Oceanographic and Meteorological Laboratory, Miami, Florida, USA

Abstract Analysis of Bay of Bengal tropical cyclone (TC) track data for the months of May–June during 1979–2014 reveals a meridional dipole in TC intensification: TC intensification rates increased significantly in the northern region and decreased in the southern region. The dipole is consistent with changes in the large-scale TC environment estimated using the Genesis Potential Index (GPI) for the same period. While an increase in lower troposphere cyclonic vorticity and midtroposphere humidity in the northern Bay of Bengal made the environment more favorable for TC intensification, enhanced vertical wind shear in the southern Bay of Bengal tended to reduce TC development. These environmental changes were associated with a strengthening of the monsoon circulation for the months of May–June, driven by a La Niña-like shift in tropical Pacific SSTs and associated tropical wave dynamics. Finally, analysis of a suite of climate models from the Coupled Model Intercomparison Project Phase 5 archive shows that most models correctly reproduce the link between ENSO and premonsoon Bay of Bengal TC activity at interannual timescales, demonstrating the robustness of our main conclusions.

1. Introduction

Tropical cyclones (TCs) are among the most destructive, persistent, and recurrent natural hazards in the global tropics and subtropics with widespread impacts [*Emanuel*, 2003]. A significant majority of the deadliest TCs in recorded history have occurred in the Bay of Bengal [*Frank and Husain*, 1971]. This is surprising given that only about three to four TCs form annually in this semienclosed basin [*Alam et al.*, 2003]. However, a combination of factors such as a flat coastal terrain and high population density of surrounding nations causes TCs in the Bay of Bengal to have devastating consequences upon landfall [*Islam and Peterson*, 2009].

The annual cycle of TCs in the northern Indian Ocean displays a distinct bimodal structure [*Li et al.*, 2013]. The TC season begins in April, as the sea surface temperatures (SSTs) rise, and continues to intensify through May. However, by the end of May and in early June, the monsoon sets in and the associated strong vertical wind shear, cooler SSTs, and unfavorable atmospheric vorticity severely limit the formation of TCs from June to September [*Li et al.*, 2013]. In October, the TC activity increases again, reaching a second peak during the month of November. While more TCs form during the postmonsoon months, the most intense storms have formed during the premonsoon period. Large ocean heat content and strong variability of northward propagating intraseasonal oscillations [*Madden and Julian*, 1972] during April–May are primarily responsible for the formation of intense TCs during the premonsoon season [*Li et al.*, 2013]. A notable example of an intense premonsoon TC is Nargis, a storm that reached an intensity of category 4 on the Saffir-Simpson scale in May 2008 and caused catastrophic destruction in Myanmar, with fatalities exceeding 130,000 [*Webster*, 2008; *Fritz et al.*, 2009; *Lin et al.*, 2009; *McPhaden et al.*, 2009].

A statistical analysis of historical TC data during the satellite period (1981–2006) showed that the intensity of the strongest TCs had increased substantially over the northern Indian Ocean [*Elsner et al.*, 2008]. However, in that study, TCs in the Bay of Bengal and the Arabian Sea were grouped together. A later study found that Bay of Bengal TCs in the postmonsoon season increased in intensity over the past 30 years and identified large-scale changes in ocean-atmosphere conditions that were responsible [*Balaguru et al.*, 2014]. *Wang et al.* [2013] found that TCs in the premonsoon month of May also increased in intensity after 1979 and attributed changes in TC activity to anthropogenic aerosols and greenhouse gas forcing. However, the role of natural climate variability in the observed changes in TC activity was not explored systematically. In addition, many

previous studies of interannual variability of Bay of Bengal TCs focused on the postmonsoon season. The reason is that major climate phenomena that impact global climate at interannual timescales, such as the El Niño–Southern Oscillation (ENSO) and Indian Ocean Dipole, tend to manifest more strongly during boreal late fall and winter. The large-scale ocean-atmosphere state was found to be more favorable for TC development in the postmonsoon Bay of Bengal during La Niña [*Girishkumar and Ravichandran*, 2012; *Felton et al.*, 2013; *Bell et al.*, 2014] and during the negative phase of the Indian Ocean Dipole [*Girishkumar and Ravichandran*, 2012]. However, the environmental impact on premonsoon TCs at interannual timescales is less clear.

By examining the correlation between Niño 3.4 SST anomalies and the Accumulated Cyclone Energy for the months of March–May in the premonsoon Bay of Bengal, *Felton et al.* [2013] suggested that ENSO may not have a significant influence on premonsoon Bay of Bengal TC activity. Although the impact of ENSO is stronger during boreal late fall and winter months, its influence over the large-scale ocean-atmosphere system in the northern Indian Ocean may persist until May–June. For instance, *Goswami and Xavier* [2005] show that ENSO plays a pivotal role not only in the withdrawal phase of the Indian summer monsoon but also during its onset phase. Thus, large-scale climate variability outside of the Bay of Bengal may affect premonsoon atmospheric conditions and TC activity in the Bay of Bengal. In this study, we examine changes in TC activity during the premonsoon months of May–June and identify their potential causes using a combination of observations and reanalysis data sets. We then examine these relationships using output from coupled climate models. The layout of the paper is as follows. Data, model, and methods are described in section 2. The results are described in section 3, and finally, the conclusions and discussion are provided in section 4.

2. Data, Model, and Methods

TC track data for the 36 year satellite period 1979–2014 are obtained from the U.S. Navy's Joint Typhoon Warning Center at https://metoc.ndbc.noaa.gov/JTWC/ [*Chu et al.*, 2002]. Monthly mean atmospheric relative humidity and horizontal winds, air temperature, sea level pressure, and SSTs for the months of May–June during 1979–2014 are obtained from the ERA-Interim reanalysis (http://www.ecmwf.int/en/research/climate-reanalysis/era-interim) [*Dee et al.*, 2011] and are used to compute the Genesis Potential Index (GPI) and the meridional tropospheric temperature gradient (ΔTT). In addition to atmospheric winds, monthly mean specific humidity is also used to understand changes in relative humidity. Monthly mean May–June National Centers for Environmental Prediction/National Center for Atmospheric Research (NCEP/NCAR) reanalysis atmospheric data [*Kalnay et al.*, 1996] and SST data from UK Met Office's Hadley Center [*Rayner et al.*, 2003], obtained from http://www.esrl.noaa.gov/psd/data/gridded/data.ncep.reanalysis.html and http://www.metoffice.gov.uk/hadobs/hadisst/, respectively, for the period 1948–2014 are used to validate our results based on ERA-Interim data. The monthly Niño 3.4 SST index, calculated as the SST averaged between 170°W–120°W and 5°S–5°N with the long-term mean removed, is obtained from http://www.cpc.ncep.noaa.gov/data/indices/.

Monthly mean atmospheric and SST data from 15 different coupled climate models of the "Coupled Model Intercomparison Project Phase 5" (CMIP5) and obtained from http://pcmdi9.llnl.gov/ are used to compute GPI, ΔTT, and the Niño 3.4 SST index. A list of the various models used is given in Table 1. We first use data from the 156 year historical period of 1850–2005 to examine the ability of the models to reproduce the relationships obtained from observational analysis. Next, we use data from the 95 year period 2006–2100 under the RCP8.5 global warming scenario, where the radiative forcing increases by about 8.5 W m^{-2} relative to the preindustrial forcing, to explore potential future changes in the Indian summer monsoon circulation strength for the month of May.

At a given point along a TC's track, the intensification rate is estimated as the linear regression coefficient of the maximum wind speed of the TC over a 24 h period consisting of four successive 6-hourly locations and beginning with the current location. Following *Camargo et al.* [2007], we define the GPI as

$$\mathrm{GPI} = \mathrm{Term\ 1}\ .\ \mathrm{Term\ 2}\ .\ \mathrm{Term\ 3}\ .\ \mathrm{Term\ 4} \tag{1}$$

Here Term 1 is $|10^5\eta|^{\frac{3}{2}}$, Term 2 is $(\frac{\mathrm{RH}}{50})^3$, Term 3 is $(\frac{1}{1+0.1V_{\mathrm{shear}}})^2$, and Term 4 is $(\frac{V}{70})^3$. η is the absolute vorticity at 850 hPa, RH is the relative humidity at 600 hPa, V is the potential intensity, and V_{shear} is the vertical wind shear calculated between 200 and 850 hPa. The potential intensity, a theoretical representation of the large-scale

Table 1. List of CMIP5 Models Used in Our Study

Center	Model Name
Beijing Climate Center	BCC-CSM 1.1
Canadian Centre for Climate Modelling and Analysis	CAN-ESM 2
Centre National de Recherches Mtorologiques	CNRM-CM5
Geophysical Fluid Dynamics Laboratory	GFDL-CM3
Geophysical Fluid Dynamics Laboratory	GFDL-ESM2G
Geophysical Fluid Dynamics Laboratory	GFDL-ESM2M
UK Met Office Hadley Centre	HADGEM2-CC
UK Met Office Hadley Centre	HADGEM2-ES
Institute for Numerical Mathematics	INMCM4
Institut Pierre-Simon Laplace	IPSL-CM5A-LR
Japan Agency for Marine-Earth Science and Technology	MIROC-ESM
Max-Planck-Institut für Meteorologie	MPI-ESM-LR
Meteorological Research Institute	MRI-CGCM3
National Center for Atmospheric Research	NCAR-CCSM4
Norwegian Meteorological Institute	NORESM1-M

ocean-atmosphere thermodynamic state [*Emanuel*, 1999] and a limit to the maximum possible intensity a TC may achieve under prevailing conditions at steady state, is calculated as

$$V^2 = \left(\frac{\mathrm{SST} - T_0}{T_0}\right)\frac{C_k}{C_D}(k_{\mathrm{SST}} - k) \tag{2}$$

where T_0 is the outflow temperature, C_k is the coefficient of enthalpy, C_D is the coefficient of drag, k_{SST} is the enthalpy of air in contact with seawater (J kg^{-1}), and k is the enthalpy of air in the TC's ambient boundary layer (J kg^{-1}). GPI budget analysis is performed following the method of *Li et al.* [2013]:

$$\delta\mathrm{GPI} = \sum_{i=1}^{4} \alpha\, i.\delta\mathrm{Term}\, i \tag{3}$$

where $\alpha 1 = \overline{\mathrm{Term}\,2}.\overline{\mathrm{Term}\,3}.\overline{\mathrm{Term}\,4}$, $\alpha 2 = \overline{\mathrm{Term}\,1}.\overline{\mathrm{Term}\,3}.\overline{\mathrm{Term}\,4}$, $\alpha 3 = \overline{\mathrm{Term}\,1}.\overline{\mathrm{Term}\,2}.\overline{\mathrm{Term}\,4}$, and $\alpha 4 = \overline{\mathrm{Term}\,1}.\overline{\mathrm{Term}\,2}.\overline{\mathrm{Term}\,3}$. The overbar indicates the monthly climatology and δ indicates the change from monthly climatology.

To understand changes in relative humidity (RH), we use the following relationship between relative humidity, specific humidity, and air temperature:

$$\mathrm{RH} \approx 0.263pq\left[\exp\left(\frac{17.67(T - T_{\mathrm{ref}})}{(T - 29.65)}\right)\right] \tag{4}$$

where q is the specific humidity, T is the air temperature (K), T_{ref} is 273.16, and p is the pressure (Pa) [*Bolton*, 1980]. Using a similar approach as with the GPI, we estimate the contribution of changes in air temperature and specific humidity to those in relative humidity. The horizontal and vertical moisture flux convergence is estimated as $-\nabla.(qV_h)$ and $-\frac{\partial(q\omega)}{\partial p}$, respectively, where V_h is the horizontal velocity vector and ω is the vertical velocity.

The ΔTT, a metric that represents the strength of the Indian summer monsoon circulation, is calculated following the method of *Goswami and Xavier* [2005]. We first average the tropospheric temperature vertically between 200 and 600 hPa, and then we take the difference between an area average over a northern box (40°E–100°E, 10°N–35°N) and a southern box (40°E–100°E, 15°S–10°N). We consider TC data during the 36 year satellite period of 1979–2014 in this study. Hence, for the purpose of this study, "change" is defined as the mean over the second half of this period (1997–2014) minus the mean over the first half of this period (1979–1996). Throughout this paper, "northern Bay" refers to the part of the Bay of Bengal that is to the north of 14°N, while "southern Bay" refers to the part of the Bay of Bengal that is to the south of 14°N. We chose the 14°N latitude to divide the Bay of Bengal into two since this would roughly divide the number of TC track locations equally. All correlation coefficients, unless otherwise stated, are statistically significant at the 95% level.

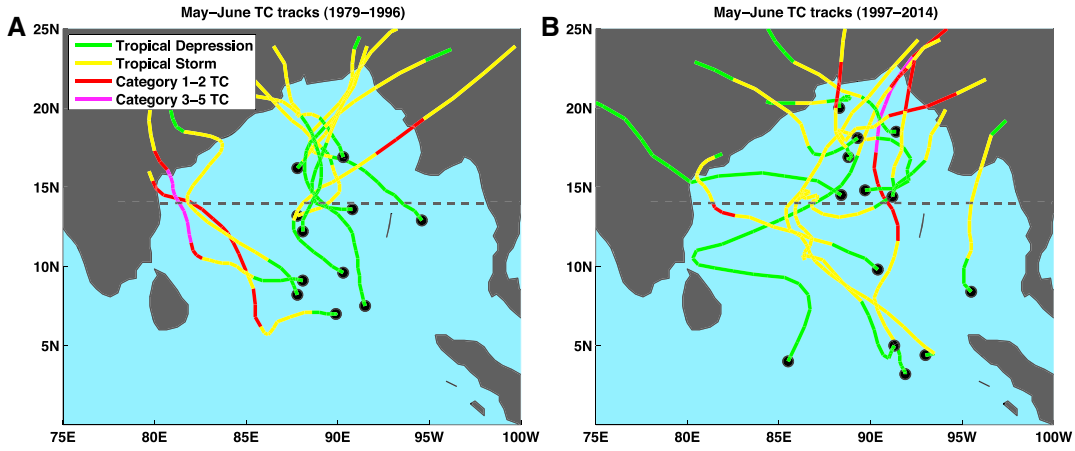

Figure 1. The tracks of Bay of Bengal TCs for the months of May–June and for the 36 year period 1979–2014. (a) The tracks from the first 18 year period 1979–1996 and (b) the tracks from the later 18 year period. The tracks are color coded based on their intensity using the Saffir-Simpson Hurricane Wind Scale: tropical depression (<17 m s^{-1})—green, tropical storm (17–33 m s^{-1})—yellow, category 1–2 TC (33–49 m s^{-1})—red, and category 3–5 TC (>49 m s^{-1})—magenta. The black dashed line approximately divides the Bay of Bengal into two halves.

3. Results

3.1. TC Track Data Analysis

The tracks of Bay of Bengal TCs for the months of May–June and for the years 1979–2014 are shown in Figure 1. During the 18 year period 1979–1996, there were two TCs in the northern Bay of Bengal that reached "tropical storm" intensity (maximum wind speed of 17–32 m s^{-1}). During the next 18 year period of 1997–2014, seven TCs formed in the northern Bay out of which three intensified into category 1 TCs. The first of these three TCs was BOB 01 during May 2004 that reached a peak intensity of 33 m s^{-1} and caused nearly 236 fatalities and tremendous damages in Myanmar. The second of the three TCs, TC Akash, caused destruction in the Andaman and Nicobar Islands and several other regions surrounding the Bay during May 2007. TC Aila was the third of the three TCs and occurred during May 2009. It caused tremendous destruction in India and Bangladesh with 300 fatalities resulting from the TC's storm surge and outbreak of diseases in its aftermath [*Momen*, 2010; *Bhunia and Ghosh*, 2011]. It must be noted that TCs that form in the northern Bay have a relatively short lifetime over the ocean before making landfall. Hence, they need to intensify rapidly in order to reach an intensity of category 1 within that short duration.

In the southern Bay of Bengal, three out of nine TCs that formed during the period 1979–1996 attained an intensity of category 1 or higher. The first was the 1979 Tamil Nadu-Sri Lanka Cyclone, a category 2 TC that affected the regions of south India and Sri Lanka, causing nearly 700 casualties. The second was the 1990 Andhra Pradesh Cyclone, a category 4 TC that caused nearly 1000 fatalities in the coastal Indian state of Andhra Pradesh, and the third was BOB 01, a category 1 TC that struck Myanmar in 1992. During the later 18 year period, three out of the six TCs that formed achieved category 1 or higher intensity. While the first of these three was BOB 01 during 1997, a category 4 TC that struck Bangladesh near Chittagong and was responsible for more than a 1000 deaths, the second and third were category 1 TCs BOB 01 during 1998 and TC Laila during 2010. Unlike TCs in the northern Bay that form and intensify in the same part of the Bay of Bengal, the intensity attained by TCs that form in the southern Bay may depend on environmental conditions in both the southern as well as the northern part of the Bay of Bengal. Hence, to understand the impact of the local environment on TCs, we examine TC intensification rates.

We consider 6-hourly TC track locations and compute the TC intensification rates at those locations. Generally, observed TC analysis in the Bay of Bengal has sample size limitations owing to the relatively small number of TCs that form in this basin. However, the analysis presented in this study is not based on the number of TCs but rather on 6-hourly TC track locations. Since we are interested in understanding the large-scale environment, we consider track locations in the northern and southern Bay irrespective of where the TC formed. Next, performing a spatiotemporal autocorrelation analysis reveals that intensification rates for TCs are correlated at 0.86, 0.57, and 0.21 with their intensification rates 6, 12, and 18 h later, respectively. In other words, less than 5% of the variance in TC intensification rates 18 h later is explained by current intensification rates.

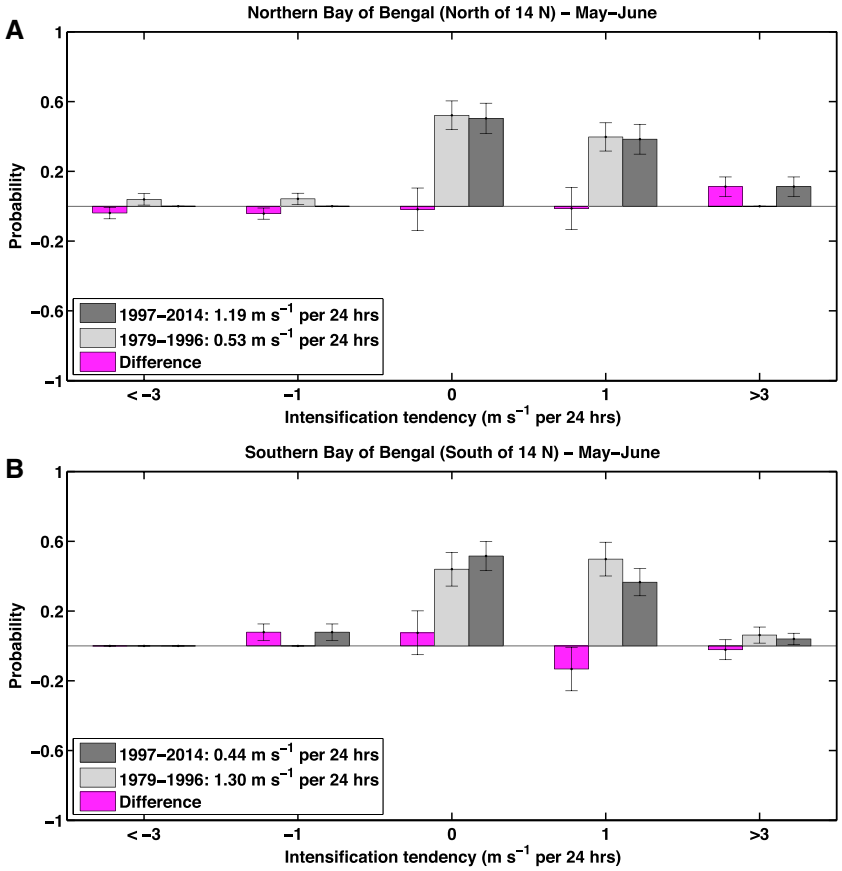

Figure 2. (a) Probability distribution functions (PDFs) of intensification rates (m s^{-1} per 24 h) and their difference, with error bars, are shown for the northern Bay. The PDF for the first 18 year period is shown in light grey, the PDF for the second 18 year period in dark grey, and their difference in pink. The mean intensification rate for each period is also indicated. (b) As in Figure 2a but for the southern Bay.

Thus, to ensure that our analysis is based on independent data samples, we subsampled TC track locations every 18 h. Note that TC track data have also been subsampled to ensure that the TC wind speed and translation speed distributions are statistically indifferent for the two 18 year periods. This minimizes the influence of other factors such as the TC's natural lifecycle and the large-scale wind on TC intensification and ensures that the results are not contaminated by sampling issues [*Balaguru et al.*, 2012]. Also, we excluded TC track locations within 24 h of landfall. After subsampling, there are 25 TC track locations in the northern Bay for the period 1979–1996 and 26 for the period 1997–2014. In the southern Bay, there are 32 and 25 TC track locations for the first and second 18 year periods, respectively. These sample sizes are adequate to obtain statistical significance for TC intensification rate changes based on a Student's *t* test for difference of means.

We generate the probability distribution function (PDF) of intensification rates for each 18 year period. The probability distribution functions (PDFs) were estimated using the "Monte Carlo" method of repeated random sampling [*Balaguru et al.*, 2012]. Figure 2a shows PDFs of intensification rates for the northern Bay and their difference. The PDF for the period 1997–2014 is skewed to the right when compared to the PDF for the period 1979–1996. This indicates that TCs intensified more strongly in the northern Bay during the latter half of the 36 year period compared to the first half. The mean intensification rate for TCs in the northern Bay is 1.19 m s^{-1} per 24 h during the period 1997–2014, while the mean intensification rate for the period 1979–1996 is about 0.53 m s^{-1} per 24 h. This difference is statistically significant at the 95% level based on a Student's *t* test for difference of means. These results firmly suggest that TC intensification rates increased in the northern Bay during the period 1997–2014.

The PDFs of intensification rates for each 18 year period and their differences are shown in Figure 2b for the southern Bay. Compared to the northern Bay, the shift in the PDFs in the southern Bay is in the opposite

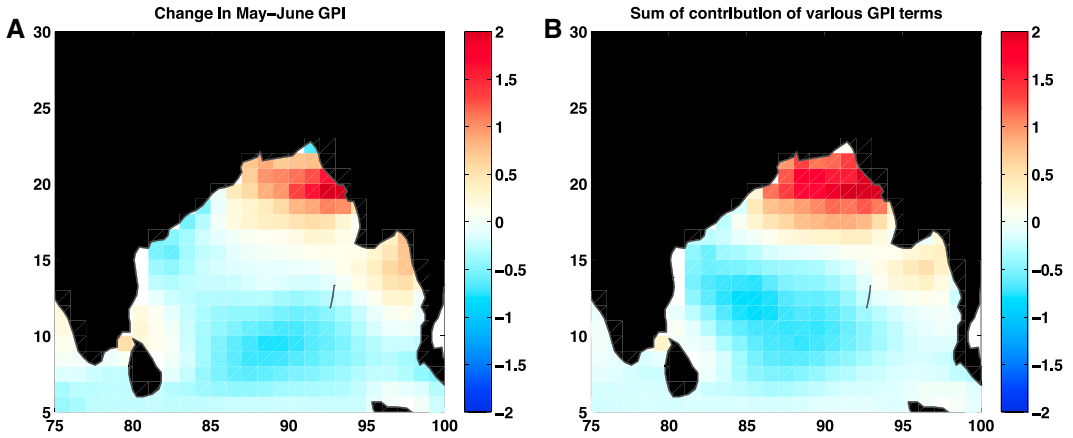

Figure 3. (a) Change in GPI (difference between GPI averaged over the periods 1997–2014 and 1979–1996), averaged over the months of May–June. (b) Change in GPI estimated indirectly as the sum of contributions of individual terms.

direction. The PDF for the period 1997–2014 is skewed to the left when compared to the PDF for the period 1979–1996, indicating that TC intensification rates have decreased during the latter half of the 36 year period. The mean TC intensification rate in the southern Bay for the period 1997–2014 is 0.44 m s^{-1} per 24 h, while the mean intensification rate for the period 1979–1996 is 1.30 m s^{-1} per 24 h, a difference statistically significant at the 95% level. Taken together with the results from the northern Bay, a meridional dipole-like pattern in TC intensification emerges in the premonsoon Bay of Bengal during the months of May and June. Similar results are obtained when we vary the period over which intensification rates are computed and the period over which the analysis is conducted (supporting information Figures S1 and S2). Consequently, these results are fairly robust.

3.2. GPI Analysis

Next, we attempt to understand the background environmental conditions responsible for these changes in TC activity using the GPI, a representation of the large-scale ocean-atmosphere state that plays an important role in TC development. While the GPI has traditionally been used to understand cyclogenesis [*Camargo et al.*, 2007], and more recently the genesis of monsoon depressions [*Vishnu et al.*, 2016], it has also been applied to understand TC intensification [*Girishkumar et al.*, 2014]. The GPI is of additional value for TC studies in the northern Indian Ocean, which are hampered by the relatively low annual frequency of TCs. This makes the GPI, which is not constrained by availability of TC track data, an attractive tool for this study. Figure 3a shows the difference between the mean GPI averaged over the period 1997–2014 and the mean GPI averaged over the period 1979–1996 for May–June. The changes in GPI are consistent with changes in TC activity seen previously. In the northern Bay, where TCs intensified more strongly during the latter half of the 36 year period, the GPI increased. On the other hand, in the southern Bay, where TC intensification rates decreased, the GPI decreased. This is consistent with our previous result of a meridional dipole in TC intensification rate changes. Having established that the framework of GPI is consistent with observed TC activity, we now use the GPI to further understand how each environmental factor is responsible for these changes in TC intensification.

We follow the method of *Li et al.* [2013] and compute the contribution of each term of the GPI to the total change in GPI. Though this method of separating the contribution of individual terms is based on a linear approximation, it has been shown to account for most of the observed changes in GPI [*Li et al.*, 2013]. Consider Figure 3b, which shows the sum of contributions of the various terms to the total GPI. The change in the linear approximation to GPI compares very well with the actual change in GPI shown in Figure 3a. The contribution of each individual term to the change in GPI is shown in Figure 4. There are positive contributions from low-level vorticity and relative humidity in the northern Bay (Figures 4a and 4b), while there is a weak negative contribution from low-level vorticity term and a strong negative contribution from vertical wind shear in the southern Bay (Figure 4c). Thus, the increase in GPI in the northern Bay was caused by an increase in low-level vorticity and enhanced moisture in the midtroposphere. In the southern Bay, the decrease in GPI is mainly due to an increase in vertical wind shear. We found that the potential intensity term does not contribute significantly to changes in GPI (Figure 4d). The potential intensity represents the large-scale ocean-atmosphere thermodynamic state and is heavily constrained by SST in the tropics. Although there was likely an increase

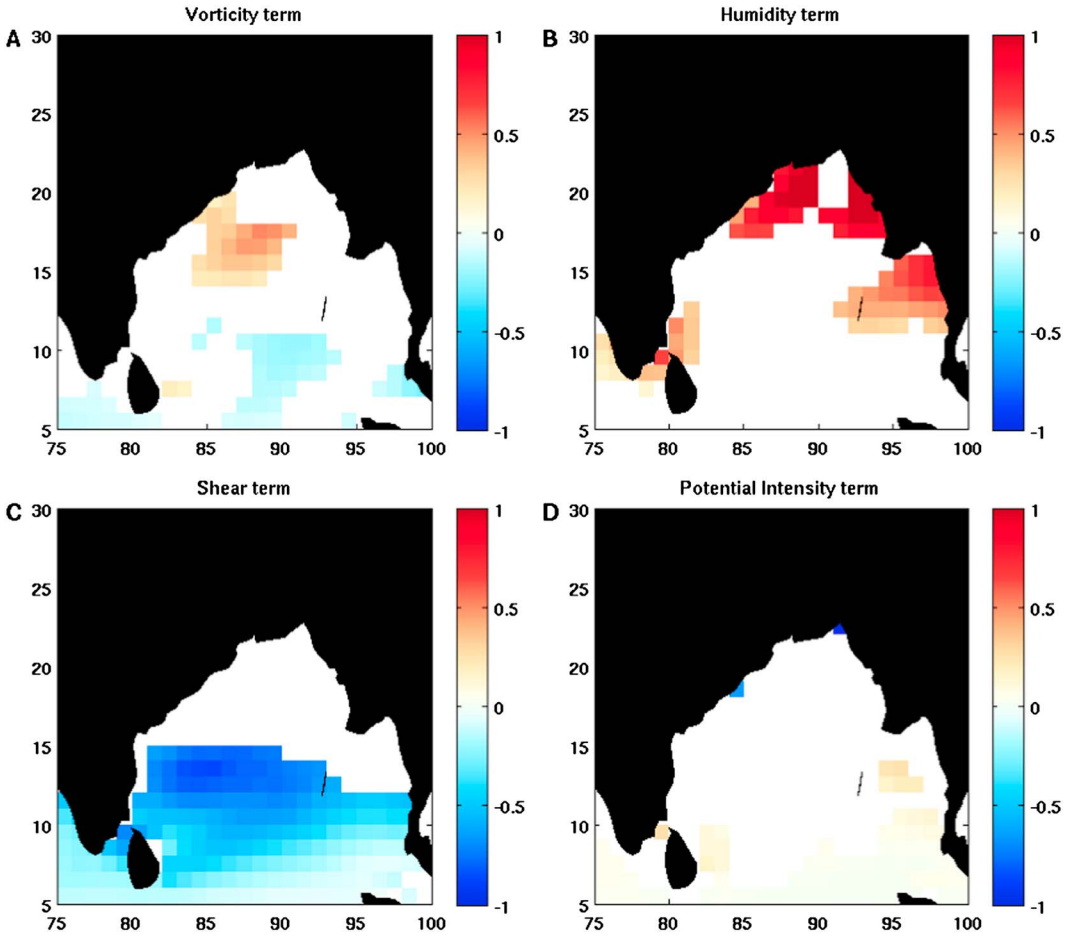

Figure 4. Contribution of various terms to the change in GPI shown in Figure 3a. (a) Low-level vorticity change, (b) midtropospheric relative humidity (600 hPa), (c) vertical wind shear, and (d) potential intensity. Changes shown are averaged over the months of May–June and are statistically significant at the 95% level.

in SST over the 36 year period [*Wang et al.*, 2013], it did not contribute significantly to changes in TC intensification.

To further understand the changes in environmental parameters, we examine changes in the large-scale circulation. Figures 5a and 5b show changes in atmospheric circulation at 850 hPa and 200 hPa, respectively, for May–June. The pattern of changes in the lower level and upper level winds indicates a strengthening of the monsoon circulation. There are anomalous southwesterlies and an anomalous anticyclonic vorticity at lower levels in the southern Bay. On the other hand, there is an anomalous cyclonic vorticity in the northern Bay at the lower levels. At upper levels, there are anomalous northeasterlies in the entire Bay with more easterly winds over the southern Bay. The combination of southwesterlies at the lower levels and northeasterlies at the upper levels gives rise to the increase in vertical wind shear in the southern Bay noted earlier (Figure 4c). The positive contribution of relative humidity to GPI (Figure 4b) suggests an increase in midtropospheric moisture in the northern Bay. Analysis of relative contributions of specific humidity and air temperature to relative humidity confirms that changes in relative humidity are dominated by changes in specific humidity (supporting information Figure S3). The sum of the horizontal and vertical moisture flux convergence change terms is shown in Figure 5c. There is enhanced moisture convergence in the northern Bay and near the southern tip of India to the east of Sri Lanka, consistent with the positive contribution of the humidity term to the GPI (Figure 4b).

The above noted changes in monsoon circulation are in agreement with the idea of an earlier monsoon onset trend observed in recent decades [*Bollasina et al.*, 2013; *Kajikawa et al.*, 2012]. To understand the cause for the enhanced monsoon circulation in May–June, we consider the change in vertically averaged May–June

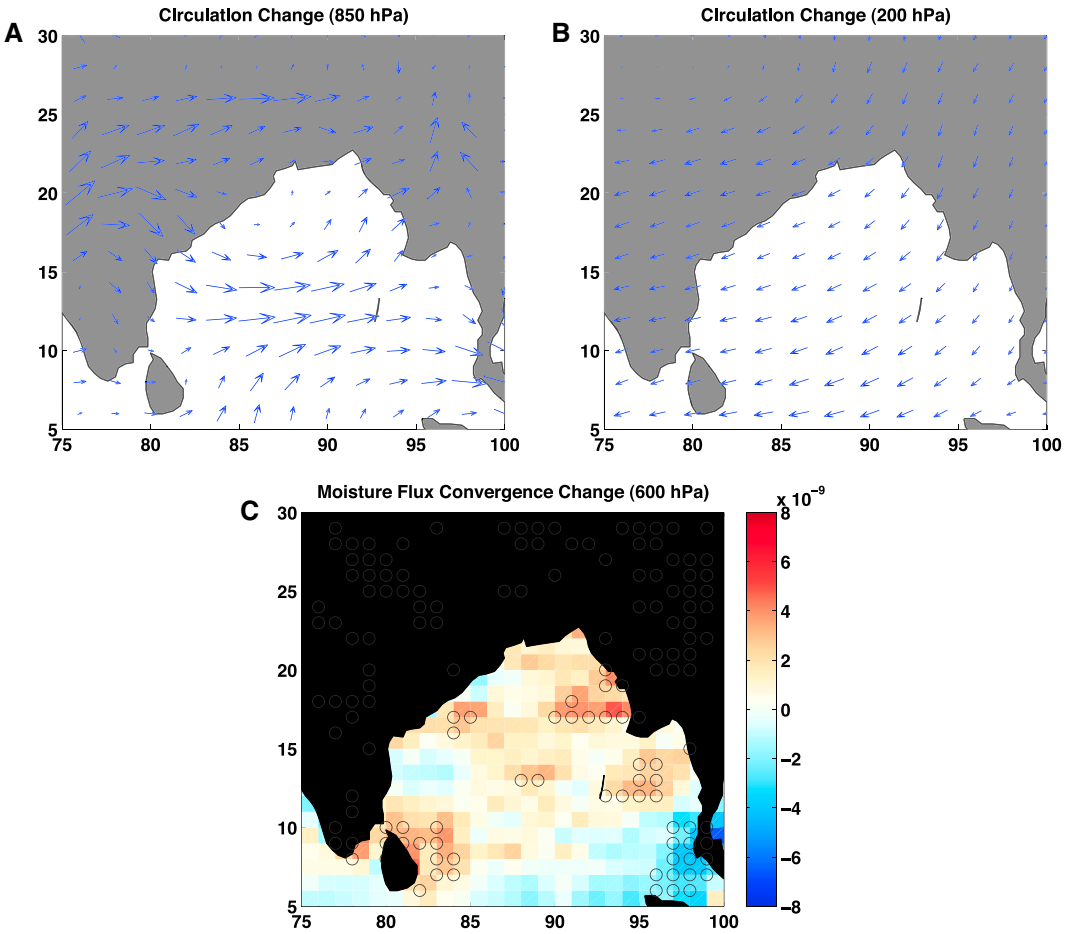

Figure 5. (a) Change in circulation at 850 hPa level. (b) Change in circulation at 200 hPa level. (c) Change in 600 hPa moisture flux convergence (kg kg^{-1} s^{-1}). Changes shown are averaged over the months of May–June, and stippling indicates statistical significance at the 95% level.

tropospheric temperature (Figure 6a). The tropospheric temperature increased considerably over the northern Indian subcontinent during 1979–2014. The enhanced heating over the northern Indian subcontinent, and the consequent increase in ΔTT, invigorated the monsoon circulation. The correlation between ΔTT and GPI is shown in Figure 6b. In the northern Bay, the correlation between ΔTT and GPI is positive, while there is a negative correlation between ΔTT and GPI in the southern Bay. This suggests that a strengthening of the monsoon circulation created a dipole in TC intensification, with the northern Bay more conducive to TC intensification and the southern Bay less favorable for TC intensification.

3.3. Understanding the Remote Influence of ENSO

Finally, we ask ourselves the following question. What caused the May–June monsoon circulation to strengthen during the latter half of the 36 year period? Figure 7a shows that the correlation between ΔTT and SST for the months of May–June resembles a La Niña-like pattern. In other words, during a La Niña, the May–June monsoon circulation gains strength. Changes in SST over the 36 year period indeed show a La Niña-like pattern in the Pacific (Figure 7b). An interesting point to note here is that besides changes in tropical Pacific SSTs, there are also changes in Indian Ocean SSTs. Specifically, there is a positive SST change in the tropical Indian Ocean. However, in Figure 7a, the correlation between ΔTT and SST is negative in the tropical Indian Ocean. Hence, the positive SST change in the tropical Indian Ocean cannot have caused the strengthening of the May–June monsoon circulation. Thus, changes in tropical Pacific SSTs played a more significant role in the May–June monsoon circulation changes.

When considering the 36 year period 1979–2014, there were more El Niño events during the first half of the period (http://www.cpc.ncep.noaa.gov/products/analysis_{m}onitoring/ensostuff/ensoyears.shtml). During the period of 1979–1996, there were seven El Niño (1982, 1983, 1987, 1991, 1992, 1993, and 1994) and

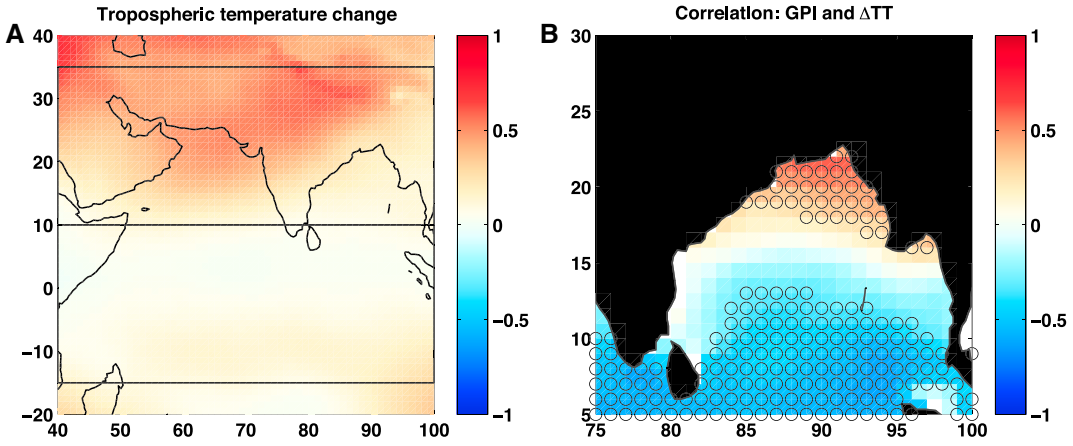

Figure 6. (a) Change in May–June tropospheric temperature, averaged between 200 and 600 hPa (°C). The two boxes indicate the regions over which the tropospheric temperature is averaged to estimate ΔTT. (b) Correlation between ΔTT (°C) and GPI, averaged over the months of May–June. Stippling indicates regions where the correlation is statistically significant at the 95% level.

three La Niña (1985, 1988, and 1989) events based on the Niño 3.4 SST index averaged over May–June. On the other hand, during the second 18 year period of 1997–2014, there were three El Niño (1997, 2002, and 2005) and two La Niña (1999 and 2000) events. This change in the number of ENSO events, responsible for the La Niña-like shift in tropical Pacific SSTs shown in Figure 7b, may have resulted from the well-known phase shift of the Pacific Decadal Oscillation from positive to negative around 1999, a shift that is linked to the global warming hiatus observed in the 2000s [*Trenberth and Fasullo*, 2013]. The scatter between the May–June ΔTT and the Niño 3.4 SST index (Figure 7c) shows that they are highly correlated at −0.65, suggesting that ENSO explains nearly 42% of the variability in the ΔTT.

The change in ΔTT over the period 1979–2014 is 0.23°C and is significant at the 90% level. When this change is computed based on only ENSO years, the change in ΔTT increases to 0.44°C and is significant at the 90% level. On the contrary, when the change in ΔTT is estimated based on non-ENSO years, the change is insignificant. These results accentuate the dominant control of ENSO over ΔTT and consequently the monsoon circulation, during the premonsoon months of May–June. While the above results were based on ERA-Interim reanalysis,

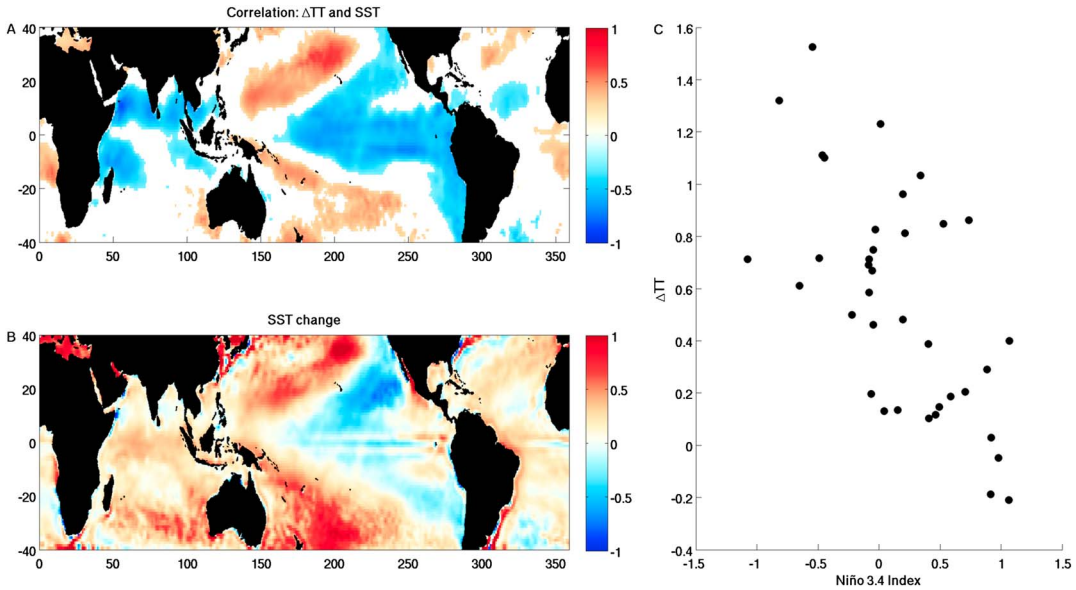

Figure 7. (a) Correlation coefficient between ΔTT and SST, averaged over the months of May–June. Values shown are significant at the 95% level. (b) Change in May–June SST (°C). (c) Scatter between Niño 3.4 SST index and ΔTT (°C), averaged over the months of May–June. The correlation coefficient is −0.65.

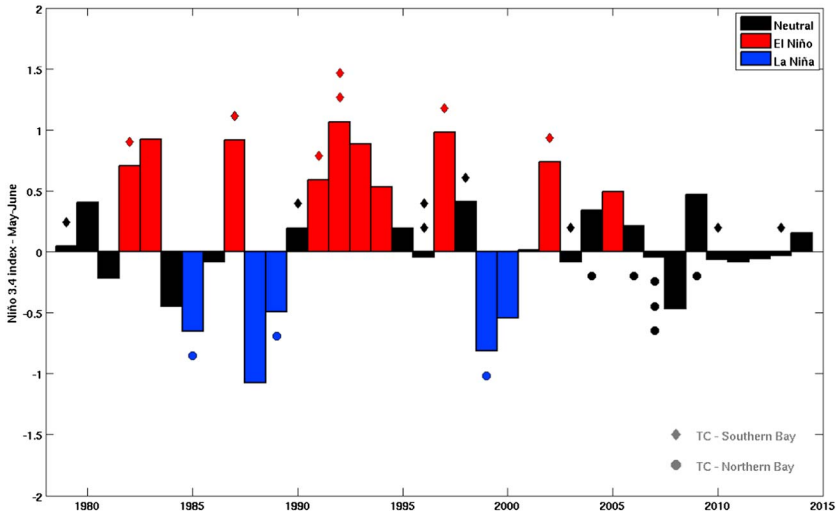

Figure 8. Impact of ENSO on May–June TC genesis in the Bay of Bengal. The bar graph represents the Niño 3.4 SST index averaged over the months of May–June. When the May–June averaged Niño 3.4 index equals or exceeds ±0.5, it is considered as an ENSO event. For each year, the formation of a TC in the northern Bay is represented by a circle and the formation of a TC in the southern Bay is represented by a diamond. The number of circles and diamonds for each year represent the number of TCs formed. The circles and diamonds are color coded based on the Niño 3.4 SST index.

a similar analysis performed using NCEP1 reanalysis for the 67 year period 1948–2014 offers further support for our conclusions (supporting information Figure S4). Examination of TC genesis further supports the importance of ENSO for premonsoon Bay of Bengal TC activity. Figure 8 shows the number of TCs that formed in the northern and southern Bay during each year along with the Niño 3.4 index. TCs form in the northern Bay only during La Niña or neutral years. On the other hand, TCs form in the southern Bay during El Niño or neutral years. The mean Niño 3.4 index when TCs form in the northern Bay is −0.12, while the mean Niño 3.4

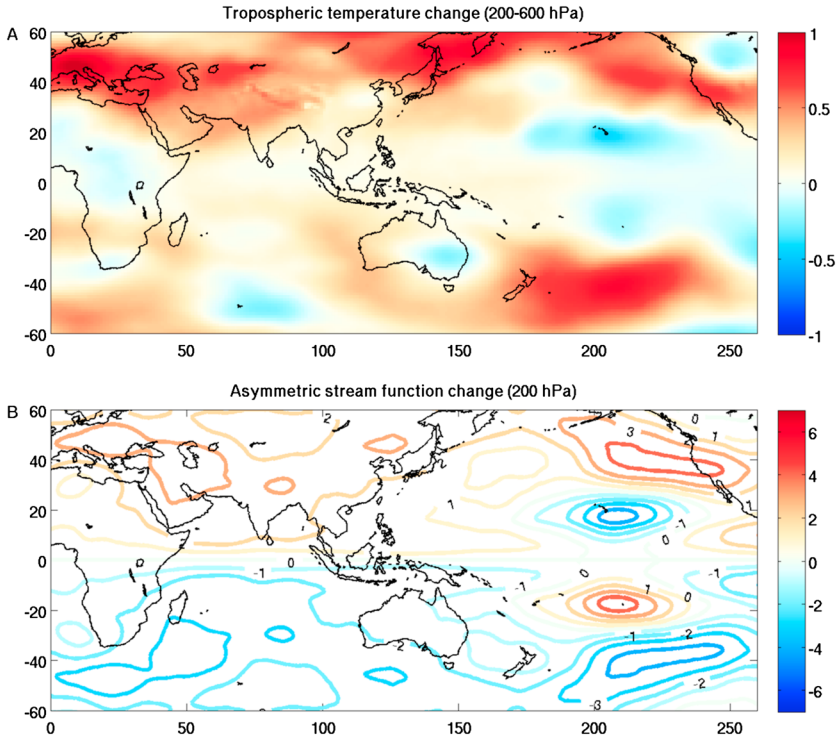

Figure 9. (a) Change in May–June tropospheric temperature (°C), averaged between 200 and 600 hPa. (b) Change in the May–June 200 hPa asymmetric streamfunction (10^6 m^2 s^{-1}).

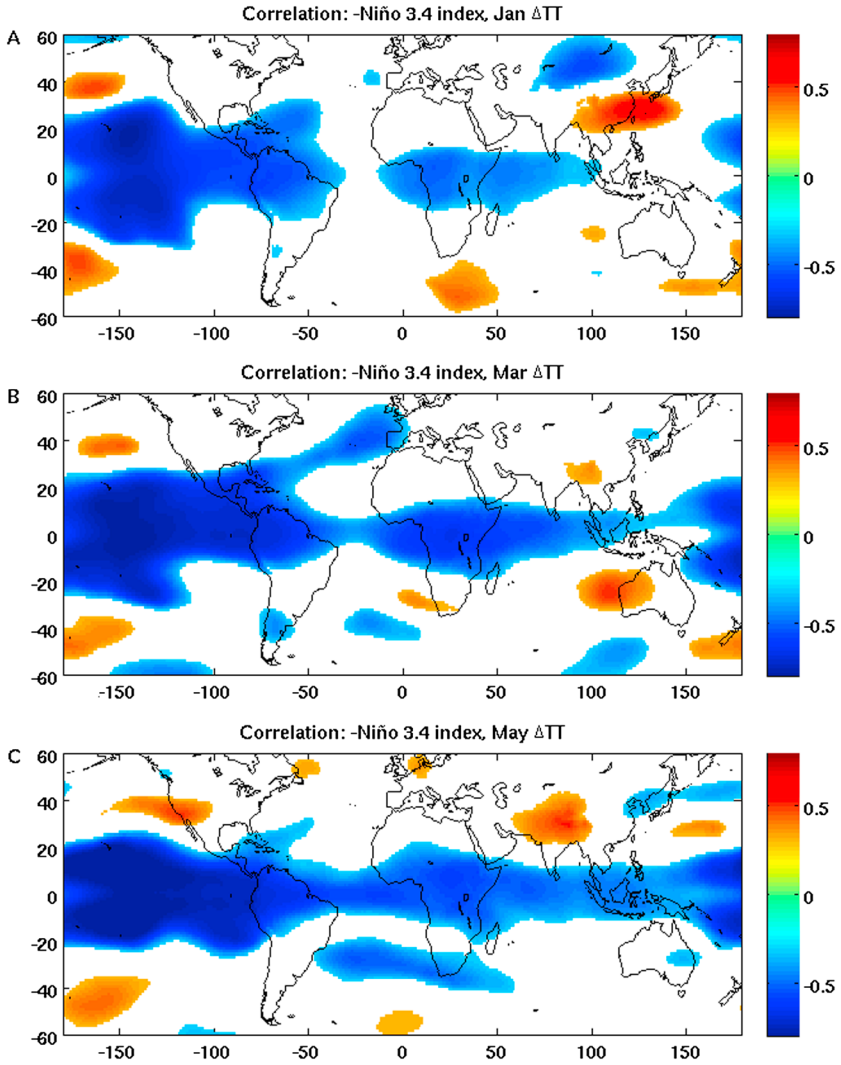

Figure 10. Correlation between the negative of the DJF Niño 3.4 SST index and tropospheric temperature (°C), averaged between 200 and 600 hPa, for the months of (a) January, (b) March, and (c) May. Values shown are statistically significant at the 95% level.

index when TCs form in the southern Bay is 0.43. This difference, statistically significant at the 95% level based on a Student's *t* test, further emphasizes the role of ENSO in the meridional dipole observed in premonsoon May–June TC activity in the Bay of Bengal.

The physical mechanisms behind the control of ENSO on summer tropospheric temperature over the Indian subcontinent are well established. The anomalous La Niña-like shift in tropical Pacific SSTs excites a wave train in tropospheric temperature that resembles a "Gill-type" response to diabatic heating in the tropics [*Rodwell and Hoskins*, 1996; *Su et al.*, 2003]. The change in May–June tropospheric temperature, averaged between 200 and 600 hPa, is shown in Figure 9a. The Rossby waves that are generated in the ENSO source region interact with the subtropical westerlies, resulting in anomalous highs and lows in the subtropics and extratropics [*Krishnan et al.*, 1998]. The quasi-stationary perturbations over the northern Indian subcontinent enhance the land-sea thermal contrast and consequently invigorate the monsoon circulation [*Goswami and Xavier*, 2005]. The change in the 200 hPa asymmetric stream function for the months of May–June, shown in Figure 9b, is consistent with the tropospheric temperature change (Figure 9a) and resembles the response to a La Niña, as shown previously [*Spencer and Slingo*, 2003].

In order to look at phase propagation of the ENSO signal, we follow *Chiang and Sobel* [2002] and examine the correlation between the negative of the December-January-February (DJF) Niño 3.4 index and the tropospheric temperature, averaged between 200 and 600 hPa, for the months of January (Figure 10a), March

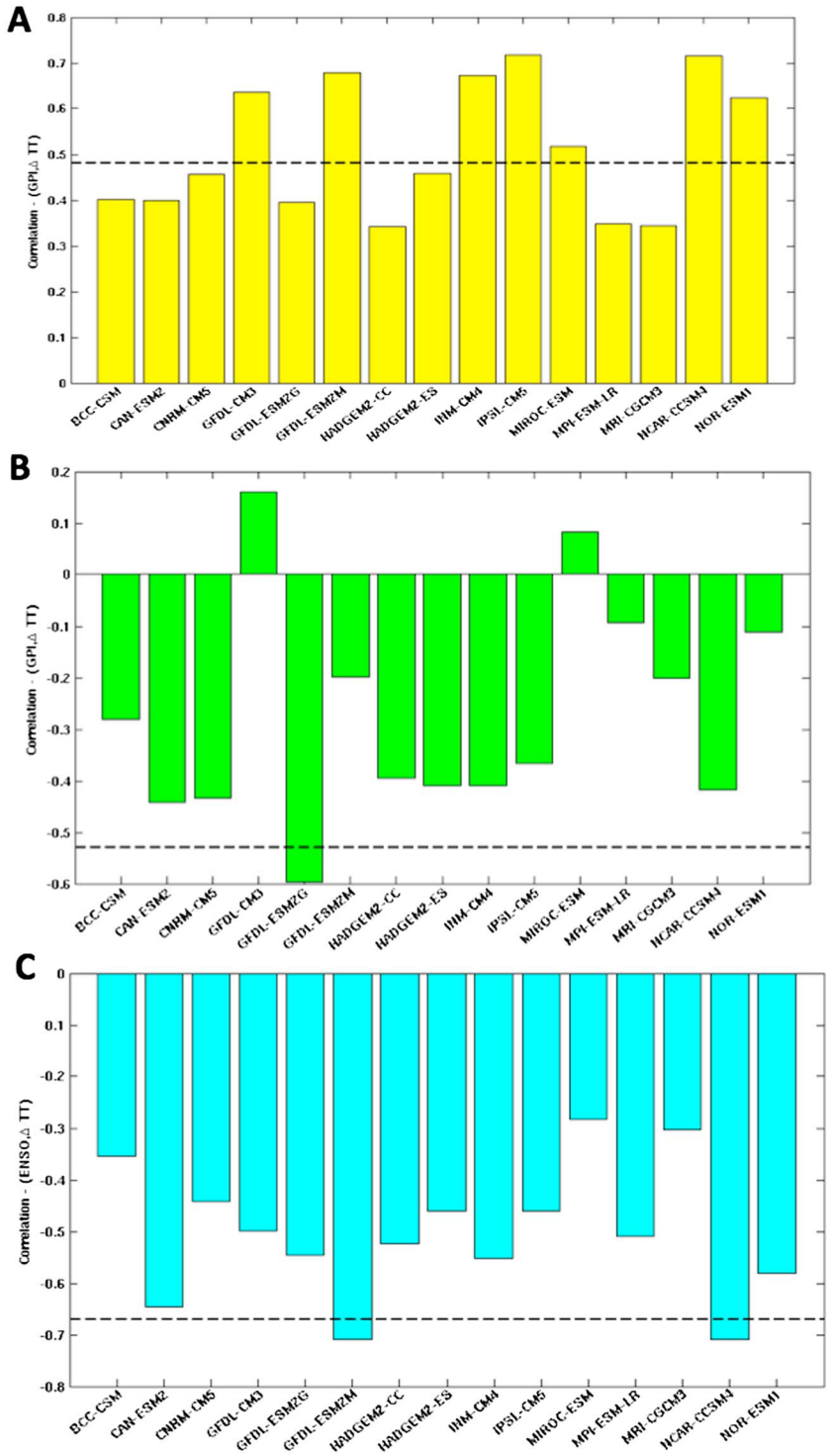

Figure 11. (a) Correlation coefficient between ΔTT and GPI averaged over the northern Bay of Bengal for the month of May and for the 156 year historical period 1850–2005 from various coupled climate models. (b) As in Figure 11a but for the southern Bay. (c) As in Figure 11a but correlation between ΔTT (°C) and Niño 3.4 SST index for the month of May. The black dashed lines indicate the corresponding correlations from observations.

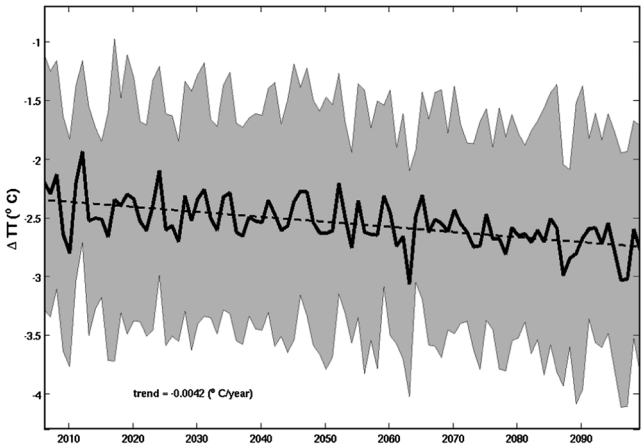

Figure 12. Multimodel ensemble mean trend in ΔTT (°C) under the RCP 8.5 global warming scenario. The trend value, statistically significant at the 95% level, is also indicated.

(Figure 10b), and May (Figure 10c). We take the negative of the Niño 3.4 SST index for ease of comparison with Figure 9a. In all three months, we see a classic dumbbell-shaped response straddling the equator in the central and eastern tropical Pacific, which is synonymous with a Rossby wave response [*Yulaeva and Wallace*, 1994]. Going from January to May, we see that the dumbbell increasingly stretches westward and carries tropospheric temperature anomalies into the tropical western Pacific and Indian Ocean regions. We speculate that the positive and negative anomalies in the subtropics result from the interaction between Rossby waves and subtropical westerlies, as noted by *Krishnan et al.* [1998]. Also, an equatorial cold tongue that develops and extends increasingly eastward is reminiscent of a Kelvin wavefront that carries tropospheric temperature anomalies eastward into the southern Bay [*Chiang and Sobel*, 2002]. These results confirm that ENSO induces a meridional dipole in the premonsoon May–June Bay of Bengal TC activity through a modulation of the monsoon circulation.

3.4. Analysis of CMIP5 Model Output

Our analysis of decadal changes in premonsoon TC activity in the Bay of Bengal reveals decadal changes in ENSO, monsoon circulation, and premonsoon Bay of Bengal TCs that are related on interannual timescales. To evaluate the ability of coupled models to reproduce the interannual relationships, we compute GPI, ΔTT and Niño 3.4 index for the 156 year historical period 1850–2005 using a suite of climate models. For this analysis, we focus on the month of May, which is the dominant month of premonsoon TC activity in the northern Indian Ocean and accounts for more than half of all TCs that form during that season in the Bay of Bengal (http://www.rsmcnewdelhi.imd.gov.in) [*Wang et al.*, 2013]. We correlate GPI averaged over the northern Bay and southern Bay with ΔTT and correlate ΔTT with the Niño 3.4 SST index. The results, shown in Figure 11, suggest that most of the models are able to reproduce these observed relationships. While the GPI averaged over the northern Bay correlates positively with ΔTT, the GPI averaged over the southern Bay generally correlates negatively with ΔTT, consistent with observations and in line with the idea of a meridional dipole. The correlation between ΔTT and the Niño 3.4 index is negative for all models, further verifying the robust control of ENSO on the May monsoon circulation, and consequently on TCs in the premonsoon Bay of Bengal.

The above analysis shows that most climate models are able to capture relationships between premonsoon TC environment, May monsoon circulation strength, and ENSO. This allows the use of models to project the future of premonsoon Bay of Bengal TC activity. Figure 12 shows the multimodel ensemble mean trend in the May monsoon circulation strength indicated by ΔTT under the RCP 8.5 global warming scenario. There is a statistically significant decreasing trend in ΔTT, suggesting that the monsoon circulation strength may decrease going into the future. These changes in monsoon circulation are argued to be forced by an El Niño-like warming pattern in tropical Pacific SSTs (not shown) [*Yeh et al.*, 2012; *Power et al.*, 2013], potentially triggered by a weakening of the Walker circulation [*Vecchi et al.*, 2008]. In light of our study, these results have potential implications for future premonsoon Bay of Bengal TC activity through the meridional dipole response to monsoon circulation changes revealed by observations and models. More specifically, they project a less favorable environment for TC intensification in the northern Bay and more favorable conditions for TC development in the southern Bay during the premonsoon months of May–June under global warming.

4. Conclusions and Discussion

Using a combination of observations and output from coupled climate models, we show in this study that the pattern of changes in premonsoon TC intensification in the Bay of Bengal over the 36 year satellite period (1979–2014) resembles a meridional dipole. While TCs have intensified faster in the northern Bay, TC intensification rates have decreased in the southern Bay over this period. Changes in GPI are consistent with the observed changes in TC activity, confirming the dipole from the standpoint of the large-scale environment. Further, a GPI budget analysis was performed to separate the relative contributions of individual terms to the total GPI change. In the northern Bay, the large-scale environment became more favorable due to an increase in low-level cyclonic vorticity and midtropospheric relative humidity. In the southern Bay, the increase in vertical wind shear made the environment less favorable.

To further understand these changes in the large-scale environment, we examined changes in atmospheric circulation. The pattern of change in winds and moisture flux convergence points to a strengthening of the May–June monsoon circulation during the latter half of the 36 year period. Further analysis reveals that the enhanced monsoon circulation is caused remotely by changes in tropical Pacific SSTs through tropical wave dynamics. Although we focus on the wave response in tropospheric temperature, anomalous tropical Pacific SSTs can also generate convective anomalies in the Intertropical Convergence Zone, which can then propagate westward as vorticity anomalies along the North African-Asian jet and cause changes in tropospheric temperature over the Asian landmass [*Shaman and Tziperman*, 2007]. A time series correlation indeed shows that ENSO exerts a significant influence on the interannual variability in the May–June monsoon circulation strength.

In this study, we examined changes in monsoon circulation and attributed them to changes in tropical Pacific SSTs and ENSO. However, SSTs and associated climate modes in the Indian Ocean may also contribute. For instance, the Indian Ocean Dipole, characterized by a large-scale zonal oscillation of SSTs in the equatorial Indian Ocean, is also known to play a role in the summer monsoon circulation [*Sankar et al.*, 2011] and to modulate the relationship between ENSO and monsoon [*Ashok et al.*, 2001]. Some other studies have attributed changes in the monsoon circulation to increasing emissions of anthropogenic aerosols [*Bollasina et al.*, 2013] or a combination of anthropogenic aerosols and greenhouse gas forcing [*Wang et al.*, 2013]. Future work is needed to more clearly understand the roles of various natural climate variability and anthropogenic forcings in monsoon circulation changes.

Finally, there are other factors that may contribute to future changes in TC activity in the Bay of Bengal that are not directly related to changes in monsoon. For example, the moisture levels in the atmosphere are projected to increase under global warming [*Held and Soden*, 2006]. Also, the northern Indian Ocean exhibits the highest warming rates among the global tropical upper oceans [*Barnett et al.*, 2005]. While the strong warming in the Indian Ocean may directly impact TC development through a modulation of the upper ocean heat content, it may indirectly affect TC activity through its influence on the land-sea thermal contrast and consequently the Indian summer monsoon circulation [*Roxy et al.*, 2015]. Thus, a complete analysis of the GPI or the large-scale TC environment is needed to accurately project future premonsoon TC activity under climate change.

Acknowledgments
This research is based on work supported by the U.S. Department of Energy (DOE) Office of Science Biological and Environmental Research as part of the Regional and Global Climate Modeling program. The Pacific Northwest National Laboratory is operated for DOE by Battelle Memorial Institute under contract DE-AC05-76RL01830. G.F. was funded by base funds to NOAA/AOML's Physical Oceanography Division. All data used to produce the results of this paper are freely available from the URLs supplied in section 2.

References

Alam, M., et al. (2003), Frequency of Bay of Bengal cyclonic storms and depressions crossing different coastal zones, *Int. J. Climatol.*, *23*(9), 1119–1125.

Ashok, K., Z. Guan, and T. Yamagata (2001), Impact of the Indian Ocean dipole on the relationship between the Indian monsoon rainfall and ENSO, *Geophys. Res. Lett.*, *28*(23), 4499–4502.

Balaguru, K., P. Chang, R. Saravanan, L. R. Leung, Z. Xu, M. Li, and J.-S. Hsieh (2012), Ocean barrier layers' effect on tropical cyclone intensification, *Proc. Natl. Acad. Sci.*, *109*(36), 14,343–14,347.

Balaguru, K., S. Taraphdar, L. R. Leung, and G. R. Foltz (2014), Increase in the intensity of postmonsoon Bay of Bengal tropical cyclones, *Geophys. Res. Lett.*, *41*(10), 3594–3601.

Barnett, T. P., D. W. Pierce, K. M. AchutaRao, P. J. Gleckler, B. D. Santer, J. M. Gregory, and W. M. Washington (2005), Penetration of human-induced warming into the world's oceans, *Science*, *309*(5732), 284–287.

Bell, R., K. Hodges, P. L. Vidale, J. Strachan, and M. Roberts (2014), Simulation of the global ENSO–tropical cyclone teleconnection by a high-resolution coupled general circulation model, *J. Clim.*, *27*(17), 6404–6422.

Bhunia, R., and S. Ghosh (2011), Waterborne cholera outbreak following Cyclone Aila in Sundarban area of West Bengal, India, 2009, *Trans. R. Soc. Trop. Med. Hyg.*, *105*(4), 214–219.

Bollasina, M. A., Y. Ming, and V. Ramaswamy (2013), Earlier onset of the Indian monsoon in the late twentieth century: The role of anthropogenic aerosols, *Geophys. Res. Lett.*, *40*(14), 3715–3720.

Bolton, D. (1980), The computation of equivalent potential temperature, *Mon. Weather Rev.*, *108*(7), 1046–1053.

Camargo, S. J., K. A. Emanuel, and A. H. Sobel (2007), Use of a genesis potential index to diagnose ENSO effects on tropical cyclone genesis, *J. Clim.*, *20*(19), 4819–4834.
Chiang, J. C., and A. H. Sobel (2002), Tropical tropospheric temperature variations caused by ENSO and their influence on the remote tropical climate*, *J. Clim.*, *15*(18), 2616–2631.
Chu, J.-H., C. R. Sampson, A. S. Levine, and E. Fukada (2002), *The joint typhoon warning center tropical cyclone best-tracks, 1945–2000*, Joint Typhoon Warning Center Ref. NRL/MR/7540-02, Pearl Harbor, HI.
Dee, D., et al. (2011), The Era-Interim reanalysis: Configuration and performance of the data assimilation system, *Q. J. R. Meteorol. Soc.*, *137*(656), 553–597.
Elsner, J. B., J. P. Kossin, and T. H. Jagger (2008), The increasing intensity of the strongest tropical cyclones, *Nature*, *455*(7209), 92–95.
Emanuel, K. (2003), Tropical cyclones, *Annu. Rev. Earth Planet. Sci.*, *31*(1), 75–104.
Emanuel, K. A. (1999), Thermodynamic control of hurricane intensity, *Nature*, *401*(6754), 665–669.
Felton, C. S., B. Subrahmanyam, and V. Murty (2013), Enso-modulated cyclogenesis over the Bay of Bengal*, *J. Clim.*, *26*(24), 9806–9818.
Frank, N. L., and S. Husain (1971), The deadliest tropical cyclone in history, *Bull. Am. Meteorol. Soc.*, *52*(6), 438–445.
Fritz, H. M., C. D. Blount, S. Thwin, M. K. Thu, and N. Chan (2009), Cyclone Nargis storm surge in Myanmar, *Nat. Geosci.*, *2*(7), 448–449.
Girishkumar, M., and M. Ravichandran (2012), The influences of ENSO on tropical cyclone activity in the Bay of Bengal during October–December, *J. Geophys. Res.*, *117*, C02033, doi:10.1029/2011JC007417.
Girishkumar, M., K. Suprit, S. Vishnu, V. T. Prakash, and M. Ravichandran (2014), The role of ENSO and MJO on rapid intensification of tropical cyclones in the Bay of Bengal during October–December, *Theor. Appl. Climatol.*, *120*(3–4), 797–810.
Goswami, B. N., and P. K. Xavier (2005), ENSO control on the South Asian monsoon through the length of the rainy season, *Geophys. Res. Lett.*, *32*, L18717, doi:10.1029/2005GL023216.
Held, I. M., and B. J. Soden (2006), Robust responses of the hydrological cycle to global warming, *J. Clim*, *19*(21), 5686–5699.
Islam, T., and R. E. Peterson (2009), Climatology of landfalling tropical cyclones in Bangladesh 1877–2003, *Nat. Hazard.*, *48*(1), 115–135.
Kajikawa, Y., T. Yasunari, S. Yoshida, and H. Fujinami (2012), Advanced Asian summer monsoon onset in recent decades, *Geophys. Res. Lett.*, *39*, L03803, doi:10.1029/2011GL050540.
Kalnay, E., et al. (1996), The NCEP/NCAR 40-year reanalysis project, *Bull. Am. Meteorol. Soc.*, *77*(3), 437–471.
Krishnan, R., C. Venkatesan, and R. Keshavamurty (1998), Dynamics of upper tropospheric stationary wave anomalies induced by ENSO during the northern summer: A GCM study, *Proc. Indian Acad. Sci. Earth Planet. Sci.*, *107*(1), 65–90.
Li, Z., W. Yu, T. Li, V. Murty, and F. Tangang (2013), Bimodal character of cyclone climatology in the Bay of Bengal modulated by monsoon seasonal cycle*, *J. Clim.*, *26*(3), 1033–1046.
Lin, I.-I., C.-H. Chen, I.-F. Pun, W. T. Liu, and C.-C. Wu (2009), Warm ocean anomaly, air sea fluxes, and the rapid intensification of tropical cyclone Nargis (2008), *Geophys. Res. Lett.*, *36*, L03817, doi:10.1029/2008GL03581.
Madden, R. A., and P. R. Julian (1972), Description of global-scale circulation cells in the tropics with a 40–50 day period, *J. Atmos. Sci.*, *29*(6), 1109–1123.
McPhaden, M., G. Foltz, T. Lee, V. Murty, M. Ravichandran, G. Vecchi, J. Vialard, J. Wiggert, and L. Yu (2009), Ocean-atmosphere interactions during cyclone nargis, *Eos Trans. AGU*, *90*(7), 53–60.
Momen, M. (2010), Bangladesh in 2009: The peril within, *Asian Surv.*, *50*(1), 157–163.
Power, S., F. Delage, C. Chung, G. Kociuba, and K. Keay (2013), Robust twenty-first-century projections of El Niño and related precipitation variability, *Nature*, *502*(7472), 541–545.
Rayner, N., D. E. Parker, E. Horton, C. Folland, L. Alexander, D. Rowell, E. Kent, and A. Kaplan (2003), Global analyses of sea surface temperature, sea ice, and night marine air temperature since the late nineteenth century, *J. Geophys. Res*, *108*(D14), 4407, doi:10.1029/2002JD002670.
Rodwell, M. J., and B. J. Hoskins (1996), Monsoons and the dynamics of deserts, *Q. J. R. Meteorol. Soc.*, *122*(534), 1385–1404.
Roxy, M. K., K. Ritika, P. Terray, R. Murtugudde, K. Ashok, and B. Goswami (2015), Drying of Indian subcontinent by rapid Indian Ocean warming and a weakening land-sea thermal gradient, *Nat. Commun.*, *6*, 7423.
Sankar, S., M. R. Kumar, and C. Reason (2011), On the relative roles of El Niño and Indian Ocean dipole events on the monsoon onset over Kerala, *Theor. Appl. Climatol.*, *103*(3–4), 359–374.
Shaman, J., and E. Tziperman (2007), Summertime ENSO–North African–Asian Jet teleconnection and implications for the Indian monsoons, *Geophys. Res. Lett.*, *34*, L11702, doi:10.1029/2006GL029143.
Spencer, H., and J. M. Slingo (2003), The simulation of peak and delayed ENSO teleconnections, *J. Clim.*, *16*(11), 1757–1774.
Su, H., J. D. Neelin, and J. E. Meyerson (2003), Sensitivity of tropical tropospheric temperature to sea surface temperature forcing*, *J. Clim.*, *16*(9), 1283–1301.
Trenberth, K. E., and J. T. Fasullo (2013), An apparent hiatus in global warming?, *Earth's Future*, *1*(1), 19–32.
Vecchi, G., A. Clement, and B. Soden (2008), Examining the tropical pacifics response to global warming, *Eos Trans. AGU*, *89*(9), 81–83.
Vishnu, S., P. Francis, S. Shenoi, and S. Ramakrishna (2016), On the decreasing trend of the number of monsoon depressions in the Bay of Bengal, *Environ. Res. Lett.*, *11*(1), 1–11.
Wang, S.-Y., B. M. Buckley, J.-H. Yoon, and B. Fosu (2013), Intensification of premonsoon tropical cyclones in the Bay of Bengal and its impacts on Myanmar, *J. Geophys. Res. Atmos.*, *118*(10), 4373–4384.
Webster, P. J. (2008), Myanmar's deadly daffodil, *Nat. Geosci.*, *1*(8), 488–490.
Yeh, S.-W., Y.-G. Ham, and J.-Y. Lee (2012), Changes in the tropical Pacific SST trend from CMIP3 to CMIP5 and its implication of ENSO*, *J. Clim.*, *25*(21), 7764–7771.
Yulaeva, E., and J. M. Wallace (1994), The signature of ENSO in global temperature and precipitation fields derived from the microwave sounding unit, *J. Clim.*, *7*(11), 1719–1736.